Communication

Effect of a High Magnetic Field on Microstructures of Ni-Based Single Crystal Superalloy During Seed Melt-Back

WEIDONG XUAN, HUAN LIU, CHUANJUN LI, ZHONGMING REN, YUNBO ZHONG, XI LI, and GUANGHUI CAO

The effects of a high magnetic field on microstructures during seed melt-back of superalloy were investigated. Experimental results indicated that the high magnetic field significantly modified the melt-back interface shape and the melt-back zone length. In addition, stray grain on the edge of sample was effectively suppressed in the high magnetic field. Based on experimental results and quantitative analysis, the above results should be attributed to the increasing temperature gradient in a high magnetic field.

DOI: 10.1007/s11663-015-0580-y

Ni-based superalloy single crystal turbine blade has been widely used in air-engines and land-based gas turbines due to its excellent high-temperature strength and creep durability. These single crystal turbine blades are usually obtained using directional solidification technique. The aims of preparing single crystal blades are to eliminate grain boundaries and to impose an elastically soft [001] orientation.[1–3] Some studies indicated that the misorientation of primary dendrite in single crystal blades is seriously deleterious to mechanical performance.[4,5] Therefore, primary dendrite orientation plays a main role in determining mechanical properties of single crystal turbine blades.[4–6] In industrial production, a single crystal casting of Ni-based superalloy is usually obtained by a grain selector method, while an off-axial orientation dendrite may be formed, which usually deviates from [001] to 12 through 15 deg because of random characteristic of grain selector during directional solidification.[7] The deviation of crystal orientation significantly affects mechanical properties. In general, the misorientation of crystal less than 10 deg is acceptable by many engineers.[7] Recently, crystal orientation is controlled through seeding technology as the seed is a single crystal with desired orientation.[1,8] However, one of major problems encountered during directional solidification is the formation of stray grains on the edge of sample from melt-back period to initial withdrawal stage.[8,9] Due to random orientations of stray grains, high-angle boundaries may be formed and lead to the decrease of mechanical properties. Therefore, many scientific researchers have investigated the formation of stray grains during directional solidification by seeding method.[1,8–17] It is found that the convex melt-back interface shape of seed induces the sudden change of local solidification conditions, which may lead to the heterogeneous nucleation of stray grains. Moreover, It is also found that the pinching-off dendrite fragments are transferred to the interface front while being subjected to thermal-solutal convection, and then stray grains are formed ahead of the dendrite tips. In order to avoid the formation of stray grains, some methods are applied, such as optimization of cooling rate[18,19] and application of spiral grain selector between the blade and the seed.[1,9] However, these methods have still not effectively solved the problem of stray grain formation.

In the recent years, with the development of superconducting magnets, a high magnetic field has been extensively used to improve material properties during solidification. Some reports show that a high magnetic field makes the solid/liquid interface change from convex to flat shape during directional solidification of Al-Cu alloys.[20,21] In addition, it is also found that a high magnetic field suppresses the natural convection of metal melt during directional solidification.[22–24] These results imply that it is possible to utilize high magnetic field to optimize microstructures and eliminate grain defects of Ni-based single crystal superalloy by seeding method.

However, there are few studies on the effect of high magnetic field on microstructure for Ni-based single crystal superalloy during seed melt-back. The aim of the current study is to investigate the effect of high magnetic field on microstructure of superalloy PWA1483 during seed melt-back. Experimental results indicated that high magnetic field modified both the melt-back interface shape and the melt-back region length. In addition, the high magnetic field effectively suppressed stray grain formation on the edge of sample.

The alloy and seed used in the current study were Ni-based single crystal superalloy PWA1483; the nominal compositions of the alloy are listed in Table I. The seed with a diameter of 4 mm and length of 30 mm was cut from a single crystal rod with [001] crystal orientation in the solidification direction, and was placed at the

WEIDONG XUAN, Materials Research Engineer, HUAN LIU, Ph.D. Student, CHUANJUN LI, Lecturer, and ZHONGMING REN, YUNBO ZHONG, XI LI, and GUANGHUI CAO, Professors, are with the State Key Laboratory of Advanced Special Steel, Shanghai University, Shanghai 200072, P.R. China. Contact e-mail: wdxuan@shu.edu.cn

Manuscript submitted August 23, 2015
Article published online January 11, 2016.

Table I. Nominal Compositions of Ni-Based Superalloy, PWA1483 Alloy, Used in Experiments

Element	Cr	Co	Mo	W	Al	Ti	Ta	C	Ni
Wt pct	12.2	9.0	1.9	3.8	3.6	4.2	5.0	0.07	bal.

bottom of crucible to avoid full melting of single crystal seed.

The directional solidification apparatus under a high magnetic field was schematically shown in Reference 25. It mainly consisted of a superconducting magnet, a Bridgman-type furnace with a withdrawal system, and a temperature controller. The superconducting magnet could produce a vertical static magnetic field with a maximum intensity up to 14 T. The furnace temperature can reach 1973 K (1700 °C) which was controlled by a temperature controller with the precision of ±1 K. The liquid Ga-In-Sn metal (LMC) pool with a water-cooling jacket was used to cool down the sample. The temperature gradient in the sample was controlled through adjusting the temperature of the furnace hot zone which was isolated from the LMC by a refractory baffle. The withdrawal velocity was controlled by a withdrawing device and could be continuously adjusted between 0.5 and 10^4 μm/s.

In the experiments, the sample was heated to a certain temperature [1773 K (1500 °C)] at a rate of 10 K/min (°C /min) and held for 5 min, which ensured that the seed was melted partly and then directionally solidified in the Bridgman apparatus by withdrawing the crucible assembly downward at a constant withdrawal velocity to observe the microstructures of seed melt-back region and dendrite growth. The Bridgman furnace was fluxed with high-purity argon to prevent samples from being oxidized. The longitudinal (parallel to the solidification direction) microstructures of samples were observed in etched condition by optical microscope to investigate the melt-back interface shape, melt-back zone length, and dendrite growth. The etchant solution was composed of $CuSO_4$ (4 g), HCl (20 ml), H_2SO_4 (12 ml), and H_2O (25 ml). Electron backscatter diffraction (EBSD) technology was employed on the longitudinal sections to evaluate the crystal orientations of samples.

Figure 1 shows the longitudinal microstructures in seed melt-back region without and with an 8 T magnetic field. It can be found that the melt-back interface shape was convex-up in the case of no magnetic field (Figure 1(a)). With an application of an 8 T magnetic field, the convex solid–liquid interface became flat, and the melt-back zone disappeared, as shown in Figure 1(b). Therefore, this means that a high magnetic field obviously changes the melt-back interface shape and the melt-back zone length during seed melt-back.

As we know, during directional solidification, macro-interface shapes are close to the distributions of temperature fields and solute in front of liquid/solid interface, convection, and flow in the liquid near the interface.[26–29] However, for the seed melt-back interface shape, the solute distribution of single crystal seed is well distributed from edge to center because the seed arises from the stable growth stage of single crystal sample. Therefore, it is inferred that in the process of seed melt-back, the melt-back interface shape depends on the convection and flow in the liquid near the interface and distribution of temperature fields in front of the liquid/solid interface.

First, let us analyze the effect of convection in the liquid near the interface on melt-back interface shape during seed melt-back. As we know, natural convection is a result of density inversion arising from temperature and solute differences during solidification. For single crystal seed, the solute distribution is well distributed from edge to center and from upper to bottom due to the seed arising from the stable growth stage of single crystal sample. Therefore, the temperature difference is responsible for the density inversion and convection in the melt-back zone. The magnitude of natural convection of metal melt is described by a nondimensional Rayleigh number, and the corresponding expression can be written as[30]

$$R_a = \frac{g\beta_T GKh^2}{\alpha v} \quad [1]$$

where g is the acceleration due to gravity, β_T is the thermal expansion coefficient, G is the temperature gradient, K is the mushy zone permeability, h is the characteristic length, and α and v are the thermal diffusivity and kinematic viscosity, respectively.

According to Eq. [1], we evaluate the Rayleigh number in the melt-back zone during seed melt-back for superalloy PWA1483 at the scale of 4 mm. Physical parameters of the Ni-based superalloy are listed in Table II. We can easily obtain the value (about 0.015) if we take the solid fraction $f_S = 0.3$. According to a report from Pollock and Murphy,[30] the Rayleigh number higher than 0.25 induces the occurrence of convection and the formation of channels and freckle defects. Present Rayleigh number (0.015) is smaller than the critical value (0.25). Consequently, the convection and freckle did not happen. According to above analyses, the change of melt-back interface shape should be attributed to the distribution of temperature fields in front of the melt-back interface.

When a high magnetic field is applied to solidification, there are two main effects of magnetic field on melt convection: One is the electromagnetic braking (EMB) effect that arises from the interaction between the moving conducting melt and magnetic field, which suppresses the natural convection.[22–24] The other is the thermoelectric magnetohydrodynamic (TEMHD) effect that derives from the interaction between thermoelectric current and magnetic field, including the thermoelectric magnetic force (TEMF) in solid phase and the thermoelectric magnetic convection (TEMC) in liquid phase.[32,33]

In the last decade, a number of investigations have been carried out theoretically[34,35] and experimentally[36,37] to

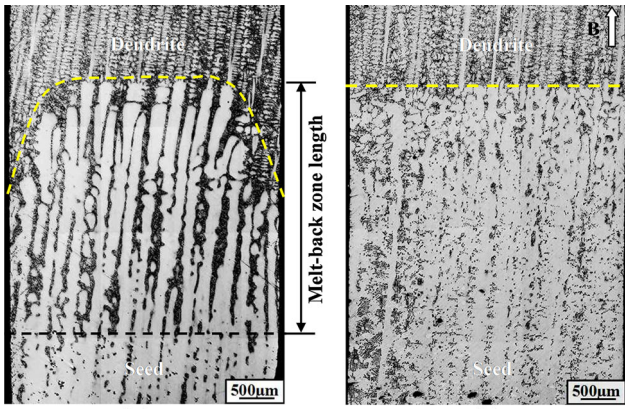

Fig. 1—(*a*) and (*b*) Longitudinal microstructures near seed melt-back region without and with an 8 T magnetic field, respectively.

study the mechanism of EMB and TEMC during solidification. Li *et al.*[38] have investigated the magnitudes of TEMC at different scales and found that the fluid velocity increases as $B^{1/2}$ in weak magnetic field and then decreases as B^{-1} in high magnetic field. When TEMC is balanced with viscous friction and EMB, the fluid velocity reaches to a maximum value. The corresponding magnetic field intensity $B_{\max}$ can be written as

$$B_{\max} = \left(\frac{\rho(S_S - S_L)G}{l\sigma}\right)^{1/3} \quad [2]$$

where ρ is the density of the alloy liquid; S_L and S_S are the thermoelectric powers of liquid and solid, respectively; l is the typical length scale, and σ is the electrical conductivity.

According to Eq. [2], the magnetic field intensity of TEMC with a maximum velocity at the scale of 4 mm is evaluated. Physical parameters of the Ni-based superalloy are presented in Table III. A magnetic field intensity of about 1.2 T is easily obtained. This calculated result implied that with further increases of magnetic field ($B \geq 1.2$ T), the EMB plays a key role in solidification process. Moreover, some studies indicate that a 2 T magnetic field effectively suppresses the convection of liquid metals.[21] Therefore, the convection has been damped totally during seed melt-back under an 8 T magnetic field. However, TEMF will appear in dendrite and increases linearly with the increasing magnetic field intensity because F_{TEMF} is directly proportional to B.[40] The corresponding expression is as follows:

$$F_{TEMF} = \frac{-\sigma_L\sigma_S f_L}{\sigma_L f_L + \sigma_S f_S}(S_S - S_L)GB \quad [3]$$

where $\sigma_L$and σ_S are the electrical conductivities of the liquid and the solid; $f_L$and f_S are the liquid and the solid fractions, respectively. Some investigations indicated that TEMF with the order of 10^5 N/m^3 is strong enough to induce the instability of solid/liquid interface[24] and break down the dendrites.[40] Therefore, the TEMF may be affecting the interface morphology and microstructure during seed melt-back.

According to Eq. [3], we evaluate the magnitude of the TEMF in dendrites under high magnetic fields. It is found that the TEMF is larger than 10^5 N/m^3 when the magnetic field is higher than 3.8 T. This means that the TEMF is strong enough to induce the instability of melt-back interface and break down the dendrites under an 8 T magnetic field. The current experimental results indicate that the stable flat melt-back interface is formed, the deformed and irregular dendrites could not be found during seed melt-back, and the well-ordered dendrite structures could form and grow into entire sample under an 8 T magnetic field (Figure 1(b)). It is also found that the melt-back zone disappears during seed melt-back under high magnetic field.

It is well known that the mushy zone length arising from the distance between the tip and the root of dendrite trunk is close to the temperature gradient, and the relationship of mushy zone length and temperature gradient under no convection has been proposed by Li *et al.*[41]. During seed melt-back, the microstructure of melt-back zone is similar to that of mushy zone.[10] Therefore, it is assumed that the melt-back zone length is equal to mushy zone length, and the corresponding expression of melt-back zone length can be expressed as

$$L = \frac{m(C_E - C_0)}{G} \quad [4]$$

where L is the melt-back zone length, m is the liquidus slope, C_0 is the initial alloy concentration, and C_E is the eutectic composition. Equation [4] shows that the melt-back zone length, L, decreases with the increasing temperature gradient. The corresponding experiment has been performed during directional solidification for Al-Si alloy.[41] It is found that the increasing temperature gradient induces the decrease of mushy zone length and protruding amplitude of the solid/liquid interface. When temperature gradient increases to a certain value, the mushy zone disappears and solid/liquid interface shape becomes flat during directional solidification. Yamaguchi *et al.*[42] report that thermodynamics constants are hardly influenced in a magnetic field with the order of 10 T. Moreover, some investigations have indicated that the high magnetic field suppresses the convection and improves the temperature gradient during solidification.[22] According to above

Table II. Physical Properties of Ni-Based Superalloy Used for Evaluation[31]

Property	Variable	Value	Unit
Thermal expansion coefficient	β_T	1.4×10^{-4}	K^{-1}
Mushy zone permeability	K*	3.66×10^{-10}	m^{-2}
Thermal diffusivity	α**	—	m^2/s
Kinematic viscosity	ν**	—	m^2/s
Solid fraction	f_S	0.3	—
Primary dendrite arm spacing	λ	300	μm
Temperature gradient	G	7000	K/m
Characteristic length	h	4	mm

* $K = K_0\frac{(1-f_s)^3}{f_s^2}$, where $K_0 = 6\times10^{-4}\ \lambda^2$.
** $\alpha\nu = 5\times10^{-12}$ m^4/s^2.[31]

Table III. Physical Parameters of the Ni-Based Superalloy[35–37,39]

Physical Parameters	Magnitude
Electrical conductivity of solid (σ_S, Ω^{-1} m^{-1}) 1327 °C	0.75×10^6
Electrical conductivity of liquid (σ_L, Ω^{-1} m^{-1}) 1327 °C	0.67×10^6
Thermoelectric power of solid (S_S, μV K^{-1}) 870 °C	–10.95
Thermoelectric power of liquid (S_L, μV K^{-1}) 1500 °C	–16
Density of liquid alloy (ρ, Kg m^{-3}), 1427 °C	7.3×10^3

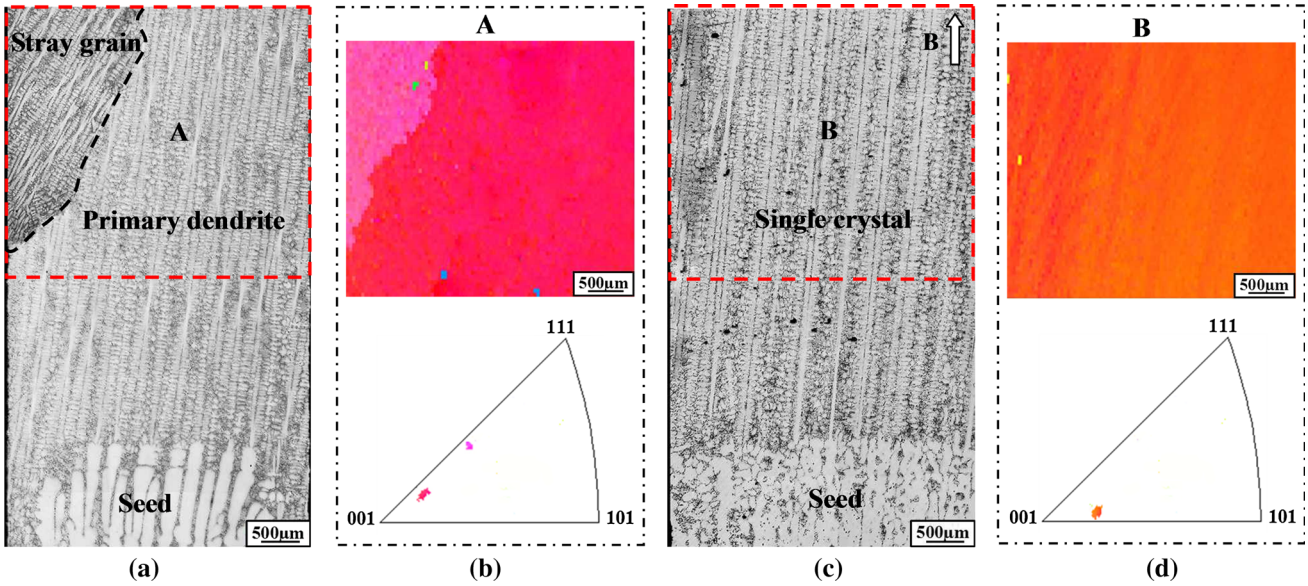

Fig. 2—(*a*) and (*c*) Longitudinal microstructures near melt-back interface for superalloy, PWA1483, without and with an 8 T magnetic field (v = 300 μm/s), respectively; (*b*) and (*d*) corresponding EBSD orientation image maps and inverse pole figures of regions A and B, respectively.

analyses, the changes of melt-back zone length and melt-back interface shape mainly depend on the effect of a high magnetic field on temperature gradient during seed melt-back. One possible explanation is that the increasing temperature gradient in melt-back interface front is due to the increasing heat transfer rate resulting from high magnetic field.[22] The temperature distribution in front of melt-back interface attains uniformity, and the length of melt-back zone becomes shorter. When the magnetic field is higher than a certain value, the melt-back zone disappears and a flat melt-back interface is formed.

Figure 2 shows longitudinal microstructures of samples in seed melt-back region of superalloy PWA483 at a withdrawal velocity of 300 μm/s without and with an 8 T magnetic field. It was observed that stray grain was formed on the edge of sample (2 mm) above melt-back region without magnetic field. However, with the application of an 8 T magnetic field, no stray grain was formed and well-ordered dendrite structures were obtained in entire sample, as shown in Figure 2(c). Furthermore, comparison of EBSD orientation maps and inverse pole figures with and without magnetic field indicated that a single crystal was obtained in the sample under a high magnetic field. Therefore, this means that a high magnetic field suppresses the formation of stray grain in the current experimental conditions.

It is well known that during directional solidification of superalloy, two primary mechanisms have been proposed for the formation of stray grains. The former is that the pinching-off of primary or secondary dendrites in mushy zone causes the formation of stray grains ahead of the dendrite tips due to the thermosolutal convection in the liquid phase.[13–17] The latter is that the heterogeneous nucleation occurs ahead of the dendrite tips, and then stray grains are formed owing to the local sudden change in the solidification conditions.[8–12]

According to the report from Stanford *et al.*,[8,9] the stray grains formation on the edge is not arising from the pinching-off dendrite fragments because these fragments are not transferred to the edge of sample during seed melt-back. Moreover, stray grains from pinching-off dendrite fragment may appear at any location of the interface front.[17,43] However, the current experimental results indicate that stray grains always appear on the edge of sample, and the nucleation position of stray grains appears very regularly compared with primary dendrites. Thus, the formation of stray grains on the edge of sample is not derived from the detachment of the fragmented dendrite. In addition, some investigations have indicated that the formation of stray grains on the edge of sample is due to local sudden change in the solidification conditions, leading to a

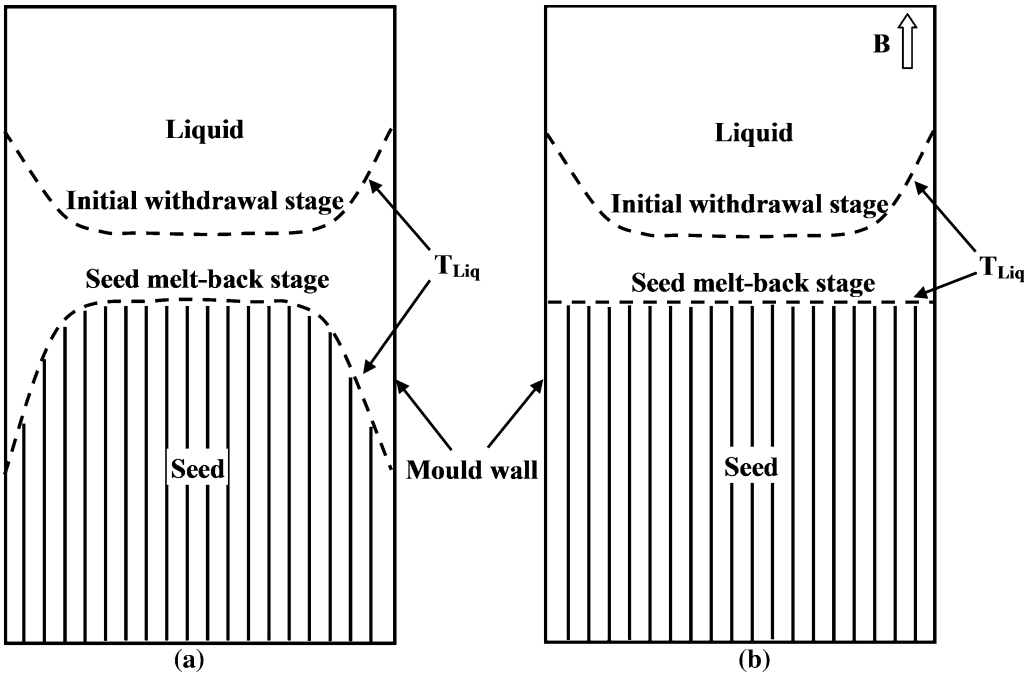

Fig. 3—(*a*) and (*b*) Schematic illustrations of the transient thermal profile from melt-back period to the initial withdrawal stage during seed melt-back without and with an 8 T magnetic field, respectively.

larger undercooling, and then heterogeneous nucleation occurs on the edge of sample.[8–12] According to above analysis, the formation of stray grains on the edge of sample should be attributed to heterogeneous nucleation.

When a high magnetic field is applied to directional solidification, the convection has been damped totally under an 8 T magnetic field. Above analyses indicate that the high magnetic field can't result in fracture of dendrite during seed melt-back. Moreover, our previous study[25] indicates that TEMF can't give rise to deformation, fracture and deflection of dendrite with a 12 T high magnetic field when the withdrawal velocity is higher than 150 μm/s. The same as no magnetic field, the formation of stray grains on the edge of sample during seed melt-back under a high magnetic field should also be attributed to heterogeneous nucleation. However, the current experimental results indicated that no stray grain was formed on the edge of sample during seed melt-back under an 8 T magnetic field. It is implied that the suppression of stray grains should be attributed to the change of undercooling on the edge of sample in a high magnetic field. It is not difficult to imagine that, during the melt-back period, the convex melt-back interface indicates higher temperature near the mold wall than in the center of the sample because the mold is heated by the furnace (Figure 3(a)). During the initial withdrawal stage, a concave isotherm is formed because the radial heat loss from the mold wall is greater than that in the center at high withdrawal velocity (300 μm/s), consequently, leads to a large undercooling near the mold wall, and then heterogeneous nucleation of stray grains becomes easy.[8,10] However, when a high magnetic field is applied to directional solidification, the convex melt-back interface shape disappears and a flat melt-back interface shape is formed due to the increasing temperature gradient in a high magnetic field. Compared with no magnetic field, during the initial withdrawal, the liquid isotherm is changed from flat to concave, the undercooling near the mold wall becomes small, and then the heterogeneous nucleation becomes difficult (Figure 3(b)). As a consequence, the high magnetic field suppresses the formation of stray grains.

In summary, the effect of a high magnetic field on microstructures was investigated experimentally during seed melt-back of superalloy. Microstructures showed that the melt-back interface shape and the melt-back zone length were obviously modified in a high magnetic field. Moreover, the high magnetic field suppressed the stray grain formation on the edge of sample. These results revealed that the increasing temperature gradient in a high magnetic field should be responsible for the change of melt-back interface shape, the disappearance of mushy zone, and the suppression of stray grains on the edge of sample during seed melt-back.

This study was supported by the Joint Funds of the National Natural Science Foundation of China (No. U1560202), the National Natural Science Foundation of China (No. 51401116), and the Shanghai Science and Technology Committee Grant (Nos. 13DZ 1108200, 13521101102, and 14521102900).

REFERENCES

1. N. D'Souza, P.A. Jennings, X.L. Yang, H.B. Dong, P.D. Lee, and M. McLean: *Metall. Mater. Trans. B*, 2005, vol. 36B, pp. 657–66.
2. M. McLean: *Directionally Solidified Materials for High Temperature Service*, The Metals Society, London, 1983, pp. 161–63.
3. D.X. Ma and A. Bührig-Polaczck: *Metall. Mater. Trans. B*, 2009, vol. 40B, pp. 738–48.
4. P. Caron, Y. Ohta, Y.G. Nakagawa, and T. Khan: *Superalloys*, S. Reichman, D.N. Duhl, G. Maurer, S. Antolovich, and C. Lund, eds., TMS, Warrendale, PA, 1988, pp. 214–24.
5. V. Sass, U. Glatzel, and M. Feller-Kniepmeier: *Acta Mater.*, 1996, vol. 44, pp. 1967–77.
6. S.S.K. Gunturi, D.W. MacLachlan, and D.M. Knowles: *Mater. Sci. Eng. A*, 2000, vol. 289, pp. 289–98.
7. P. Carter, D.C. Cox, C.A. Gandin, and R.C. Reed: *Mater. Sci. Eng. A*, 2000, vol. 280, pp. 233–46.
8. N. Stanford, A. Djakovic, B.A. Shollock, M. McLean, N. D'Souza, and P.A. Jennings: *Scripta Mater.*, 2004, vol. 50, pp. 159–63.
9. N. Stanford, A. Djakovic, B.A. Shollock, M. McLean, and N. D'Souza: *Superalloys*, K.A. Green, T.M. Pollock, H. Harada, T.E. Howson, R.C. Reed, J.J. Schirra, and S, Walston, eds., TMS, Warrendale, PA, 2004, pp. 719–26.
10. X.L. Yang, P.D. Lee, and N. D'Souza: *JOM.*, 2005, vol. 3, pp. 40–44.
11. C.B. Yang, L. Liu, X.B. Zhao, J. Zhang, D.J. Sun, and H.Z. Fu: *Appl. Phys. A*, 2014, vol. 114, pp. 979–83.
12. J.D. Miller and T.M. Pollock: *Acta Mater.*, 2014, vol. 78, pp. 23–36.
13. K.A. Jackson, J.D. Hunt, D.R. Uhlmann, and T.P. Seward: *TMS–AIME*, 1966, vol. 236, pp. 149–58.
14. T.M. Pollock, W.H. Murphy, E.H. Goldman, D.L. Uram, and J.S. Tu: in *Superalloys*, S.D. Antolovich, R.W. Stusrud, R.A. MacKay, D.L. Anton, T. Khan, R.D. Kissinger, and D.L. Klarstrom, eds., TMS, Warrendale, PA, 1992, pp. 125–34.
15. J.P. Gu, C. Beckermann, and A.F. Giamei: *Metall. Mater. Trans. A*, 1997, vol. 28A, pp. 1533–42.
16. D.X. Ma, Q. Wu, and A Bührig-Polaczck: *Metall. Mater. Trans. B*, 2012, vol. 43B, pp. 344–53.
17. H. Yasuda, I. Ohnaka, K. Kawasaki, A. Sugiyama, T. Ohmichi, J. Iwane, and K. Umetani: *J. Cryst. Growth*, 2004, vol. 262, pp. 645–52.
18. Q.Y. Xu, H. Zhang, X. Qi, and B.C. Liu: *Metall. Mater. Trans. B*, 2014, vol. 45B, pp. 555–61.
19. C. Ai, J. Zhou, H. Zhang, Y.L. Pei, S.S. Li, and S.K. Gong: *J. Alloys Compd.*, 2015, vol. 637, pp. 77–83.
20. X. Li, Y. Fautrelle, and Z.M. Ren: *Acta Mater.*, 2007, vol. 55, pp. 5333–47.
21. X. Li, Z.M. Ren, G.H. Cao, A. Gagmoud, and Y. Fautrelle: *Mater. Lett.*, 2011, vol. 65, pp. 3340–43.
22. C. Vives and C. Perry: *Int. J. Heat Mass Transf.*, 1987, vol. 30, pp. 479–96.
23. W.E. Langlois and K.J. Lee: *J. Cryst. Growth*, 1983, vol. 62, pp. 481–86.
24. W.D. Xuan, Z.M. Ren, and C.J. Li: *J. Alloys Compd.*, 2015, vol. 621, pp. 10–17.
25. W.D. Xuan, Z.M. Ren, and C.J. Li: *Metall. Mater. Trans. A*, 2015, vol. 46A, pp. 1461–66.
26. X Li, D. Zhang, Y. Fautrelle, Z.M Ren, and C. Esling: *Scripta Mater.*, 2009, vol. 60, pp. 489–92.
27. W.W. Mullins and R.F. Sekerka: *J. Appl. Phys.*, 1964, vol. 35, pp. 444–51.
28. K. Brattkus: *J. Fluid Mech.*, 1995, vol. 304, pp. 143–159.
29. L. Buhler and S.H. Davis: *J. Cryst. Growth*, 1998, vol. 186, pp. 629–47.
30. T.M. Pollock and W.H. Murphy: *Metall. Mater. Trans. A*, 1996, vol. 27A, pp. 1081–94.
31. M.C. Schneider, J.P. Gu, C. Beckermann, W.J. Boettinger, and U.R. Kattner: *Metall. Mater. Trans. A*, 1997, vol. 28A, pp. 1517–31.
32. W.J. Boettinger, F.S. Biancaniello, and S.R. Coriell: *Metall. Mater. Trans. A*, 1981, vol. 12A, pp. 321–327.
33. P. Lehmann, R. Moreau, D. Camel, and R. Bolcato: *Acta Mater.*, 1998, vol. 46, pp. 4067–79.
34. P. Lehmann, R. Moreau, D. Camel, and R. Bolcato: *J. Cryst. Growth*, 1998, vol. 183, pp. 690–704.
35. Y.Y. Khine and S. Walker: *J. Cryst. Growth*, 1998, vol. 183, pp. 150–58.
36. P. Dolda, F.R. Szofranb, and K.W. Benz: *J. Cryst. Growth*, 2006, vol. 291, pp. 1–7.
37. H. Yasuda, T. Yoshimoto, T. Mizuguchi, Y. Tamura, T. Nagira, and M. Yoshiya: *ISIJ Int.*, 2007, vol. 47, pp. 612–18.
38. X. Li, Y. Fautrelle, and Z.M. Ren: *Acta Mater.*, 2007, vol. 55, pp. 3803–13.
39. G. Pottlacher, H. Hosaeus, B. Wilthan, E. Kaschnitb, and A. Seifter: *Thermochim. Acta*, 2002, vol. 382, pp. 255–67.
40. X. Li, Y. Fautrelle, K. Zaidat, A. Gagnoud, Z.M. Ren, R. Moreau, Y.D. Zhang, and C. Esling: *J. Cryst. Growth*, 2010, vol. 312, pp. 267–72.
41. X. Li, D.F. Du, A. Gagnoud, Z.M. Ren, Y. Fautrelle, K. Zaidat, and R. Moreau: *Metall. Mater. Trans. A*, 2014, vol. 45A, pp. 5584–600.
42. M. Yamaguchi and Y. Tanimoto: *Magnetic-Science (Magnetic Field Effects on Materials: Fundamentals and Applications)*, Springer, Berlin, 2006, pp. 17–18.
43. R.H. Mathiesen and L. Arnberg: *Mater. Sci. Eng. A*, 2005, vols. 413–414, pp. 283–87.